

# TEACHER-STUDENT NETWORK FOR REAL-WORLD FACE SUPER-RESOLUTION WITH PROGRESSIVE EMBEDDING OF EDGE INFORMATION

Zhilei Liu\*, Chenggong Zhang

College of Intelligence and Computing, Tianjin University, Tianjin, China

## ABSTRACT

Traditional face super-resolution (FSR) methods trained on synthetic datasets usually have poor generalization ability for real-world face images. Recent work has utilized complex degradation models or training networks to simulate the real degradation process, but this limits the performance of these methods due to the domain differences that still exist between the generated low-resolution images and the real low-resolution images. Moreover, because of the existence of a domain gap, the semantic feature information of the target domain may be affected when synthetic data and real data are utilized to train super-resolution models simultaneously. In this study, a real-world face super-resolution teacher-student model is proposed, which considers the domain gap between real and synthetic data and progressively includes diverse edge information by using the recurrent network’s intermediate outputs. Extensive experiments demonstrate that our proposed approach surpasses state-of-the-art methods in obtaining high-quality face images for real-world FSR.

**Index Terms**— Super-resolution, Face hallucination, Facial priors, teacher-student network, edge prior

## 1. INTRODUCTION

Face super-resolution (FSR), also known as face hallucination, aims to reconstruct high-resolution (HR) face images from their degraded low-resolution (LR) counterparts. It is difficult for FSR to construct a super-resolved image from a very low-resolution image (eg.  $16\times 16$ ) since facial components are distorted. To promote the performance of FSR, recent works [1, 2, 3] integrated facial landmarks and component maps into the FSR problem to enhance FSR performance. Despite the fact that certain techniques, such as bicubic interpolation downsampling, have produced acceptable results on LR photos, the degradation of low-resolution images in real-world scenarios is typically more difficult. These SR networks trained on synthetic datasets usually lead to undesired strong artifacts in their SR results when applied to real images. As a result, attempts to solve the real-world SR problem have been made during the past few years [4, 5, 6, 7]. Specifically, Bulat et al. [4] proposed LR-GAN which uses a "high-to-low" branch network to learn

the real degradation process of real-world LR images. The methods of GLEAN [8] and GFPGAN [9] achieve promising performance for FSR with implicit priors encapsulated in a pre-trained GAN, in which complicated degradation models or training networks are investigated to simulate the actual deterioration process. Unfortunately, the performances of these approaches are still constrained by the domain gap between synthetic LR images and real LR images [6]. To tackle the real-world image SR problem, Wei et al. [6] proposed a domain-distance aware super-resolution approach that assigns different weights to various data based on the domain distance. Hou et al. [7] used three independent branches to learn the forward and backward cycle-consistent reconstruction processes to alleviate the domain gap between unpaired LR and HR face images. However, when synthetic data and real data are used to train super-resolution models at the same time, the semantic feature information of the target domain may be damaged due to the existence of the domain gap. Moreover, most of the existing real-world FSR methods usually ignore facial prior information.

To solve these problems mentioned above, we propose a teacher-student network for real-world face super-resolution with progressive edge information embedding. In accordance with prior work [10], we synthesize pseudo-paired data using a degraded network to discover the real degradation process, and then employ these data to train a teacher super-resolution network (TNet). Because of the domain gap between the synthetic data and the real data, we only use real low-resolution images to train a student super-resolution network (SNet). Existing approaches often use the cycle learning scheme to tackle super-resolution tasks when there are no paired data [11]. However, because only adversarial loss is supported in high-resolution space, the generated face image frequently suffers structural deformation. Therefore, we use the teacher-student framework to generate pseudo high-resolution images for real low-resolution images to assist in the reconstruction of face structure and maintain pixel-level accuracy in the student network. The low-frequency and high-frequency components of a single picture may usually be identified intuitively. The goal of the SR task is to restore the high-frequency component of the image, which is essential for constructing the object’s structure. In this paper, we propose to use the edge information of the face to enhance

\*Corresponding author, Email: zhileiliu@tju.edu.cn

the restoration of the global shape and local details in the reconstruction process of the face image combined with the traditional image processing method. Moreover, to improve the recovery of edge information, we employ a recurrent convolutional network as the SR backbone and progressively embed various edge information at different stages.

## 2. PROPOSED METHOD

### 2.1. Overviews

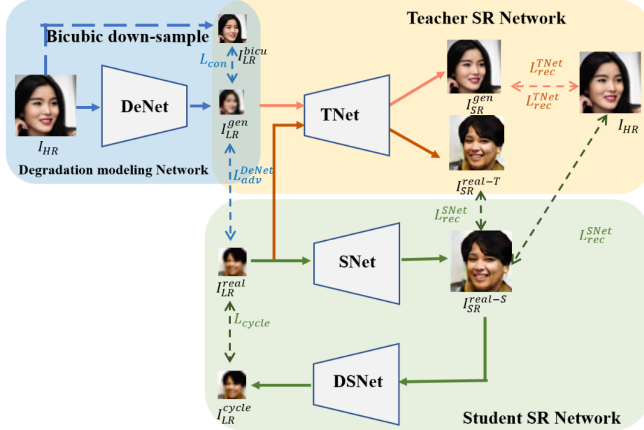


Fig. 1. Pipeline of our proposed method.

For real-world FSR, the data that can be obtained are usually two sets of unpaired LR images  $I_{LR}$  and HR images  $I_{HR}$ . To achieve real-world FSR, a two-stage framework following DASR [6] is proposed, and the overall pipeline is shown in Fig. 1. First, a degradation modeling Network (DeNet) is trained to generate an LR image  $I_{LR}^{gen}$  that conforms to the real LR domain distribution as much as possible. Then, the generated LR-HR image pairs are used to train our Teacher super-resolution Network (TNet). Different from the previous method, we fully consider the domain gap between the synthetic LR image and the real LR image and design a Student Network (SNet) to be specially used for the super-resolution reconstruction of the real LR domain image  $I_{LR}^{real}$ . Because there are no HR images corresponding to the real LR image, we use the  $I_{SR}^{real-T}$  obtained by TNet to help SNet maintain facial features and pixel-level accuracy during training. Using the data synthesized by DeNet, the results of TNet trained in a supervised manner have a better recovery of face features, so it can be used to promote the convergence of SNet during the training phase. In addition, we also use a Down-Sampling Network (DSNet) to downsample  $I_{SR}^{real-S}$  to the LR domain to use cycle consistency constraints in the LR domain to better train the SNet.

The adversarial loss can make the generated image more realistic perceptually, so all the networks are trained in an adversarial learning manner. DeNet, TNet, SNet, and DSNet are the generators of each generative adversarial network, and the structure of the discriminator adopts LightCNN [12]. For ease of representation, all discriminator parts are omitted in

Fig. 1. We retain SNet around there for experimental network verification during testing.

### 2.2. Network Architecture

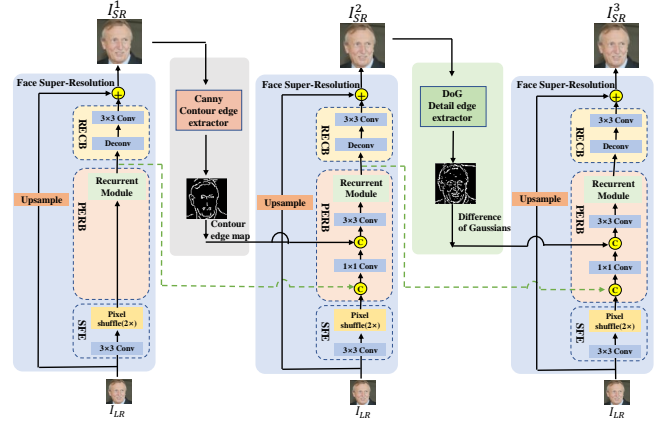


Fig. 2. The unfolded architecture of TNet and SNet. “C”, “+”, and “ $\times$ ” denote concatenation, addition, and multiplication, respectively. The green dotted lines represent feedback connections. For simplicity, we omit the activation function layer in the pipeline.

**DeNet and DSNet:** DeNet takes the HR image as input, uses a convolutional layer and 16 residual blocks [13] to extract features in high-resolution space, and then uses a downsampling layer containing two convolutional layers with a stride of 2 to reduce the spatial resolution of the features to the required size, and finally, the features are mapped back to the image domain through a convolutional layer. The network structure of DSNet is the same as that of DeNet.

**SR Network:** As shown in Figure 2, our proposed TNet and SNet can be unfolded into 3 iterations. The face super-resolution branch in each iteration contains three parts: a shallow feature extractor (SFE), a prior embedded recurrent block (PERB), and a high-resolution reconstruction block (RECB). Given a low-resolution (LR) input  $I_{LR}$ , we use a  $3 \times 3$  convolutional layer and a pixel shuffle layer to extract shallow feature  $F_{sf}^t$  at  $t$ -th iteration. Then, we use a  $1 \times 1$  and a  $3 \times 3$  convolutional layer to fuse shallow feature  $F_{sf}^t$ , the feedback feature  $F_{fb}^{t-1}$  from the previous iteration and prior information  $F_{prior}$ , and use a recurrent module to generate high-level representations  $F_{fb}^t$ . Specifically, the architecture of the recurrent module follows the feedback block in [14] and we remove its first convolutional layer. Note that there is no prior information and hidden state at the first iteration in our model. Then, the outputs of the PERB are used as the input to the RECB to generate an SR residual image of the HR face  $I_{Res}^t$ . RECB consists of a deconvolutional layer and a  $3 \times 3$  convolutional layer. Finally, the restored SR image at the  $t$ -th iteration can be described as:

$$I_{SR}^t = I_{Res}^t + H_{UP}(I_{LR}), \quad (1)$$

where  $H_{UP}(\cdot)$  denotes a bilinear upsampling operation. Therefore, we will get totally 3 SR images ( $I_{SR}^1, I_{SR}^2, I_{SR}^3$ )

for every LR image  $I_{LR}$ .

**Edge Detector:** LR images in real scenes are often affected by noise, so we choose to use the Canny edge detector that can handle noise well to extract the high-frequency edge part of the overall contour of the image. In addition, the Laplace of Gaussian function (LoG) can obtain the local details of the image, but LoG needs to perform the second-order difference or second-order partial derivative of the discrete digital image, and the calculation amount is relatively large. The Difference of Gaussians (DoG) of different scales can be used as an approximate representation of LoG. Therefore, we choose to use the Canny edge detector to extract the global contour edge of the face image from the output of the first iteration and input it into the next step to splicing with the feature map in the backbone network to promote the restoration of facial structure. And then use the DoG operator to extract the differential detail edge map of the image in the output of the second iteration, and input it into the third iteration to further promote the recovery of high-frequency information of local details of the face.

### 2.3. Loss functions

For the DeNet, in order to make the generated LR image consistent with the content of the HR image, we use the content loss to constrain the content between  $I_{LR}^{gen}$  and  $I_{LR}^{bic}$  obtained by bicubic downsampling from the HR image, which is defined as follows:

$$L_{con} = \mathbb{E} \| I_{LR}^{gen} - I_{LR}^{bic} \|_1 \quad (2)$$

To achieve the conversion to the real LR domain, we apply an adversarial loss between  $I_{LR}^{real}$  and  $I_{LR}^{gen}$ , which is defined as follows:

$$L_{adv}^{DeNet} = \mathbb{E} [\log(D(I_{LR}^{real}))] + \mathbb{E} [\log(1 - D(I_{LR}^{gen}))] \quad (3)$$

Therefore, the overall loss function of DeNet is:

$$L_{DeNet} = \alpha_1 L_{con} + \beta_1 L_{dis_1} \quad (4)$$

where  $\alpha_1, \beta_1$  are trade-off parameters. For TNet, we use LR-HR data pairs synthesized by DeNet to train in a supervised manner. To achieve better optimization, TNet uses reconstruction loss  $L_{dis_2}$  as:

$$L_{rec}^{TNet} = \mathbb{E} \left[ \frac{1}{N} \sum_{n=1}^N \| I_{HR} - I_{SR}^n \|_2^2 \right], \quad (5)$$

and adversarial loss  $L_{adv}^{TNet}$  is similar with Eq. 4 Therefore, the total loss function when training TNet is:

$$L_{TNet} = \alpha_2 L_{rec}^{TNet} + \beta_2 L_{adv}^{TNet} \quad (6)$$

For SNet, we fully consider the domain gap and only use the real LR images to train SNet. We use the pseudo HR images generated by TNet as the corresponding real LR image for supervision to guide SNet to better optimize and converge, constrained using a content loss  $L_{rec}^{SNet}$  similar with Eq. 5

In addition, in order to further promote the reconstruction of real LR images, we adopt the idea of CycleGAN [11], and introduce DSNet to impose cycle consistency constraints on LR images:

**Table 1.** Quantitative comparison with state-of-the-art methods on two synthetic datasets. The best and second best results are marked with **bold** and underline respectively, where “\*” indicates that the method indicators come from SCGAN [7], “-” indicates that the corresponding result is not listed in SCGAN, the same below.

Methods	LS3D-W balanced				FFHQ			
	FID↓	LPIPS↓	PSNR↑	SSIM↑	FID↓	LPIPS↓	PSNR↑	SSIM↑
Bicubic	271.86	0.349	23.25	0.6723	276.67	0.377	20.68	0.6525
DASR[6]	115.84	0.360	23.06	0.6594	113.01	0.398	20.72	0.6251
Real-ESRGAN*[5]	57.20	0.114	-	-	43.75	0.336	-	-
LRGAN[10]	25.35	0.241	21.70	0.6810	15.30	0.296	20.96	0.6496
GFPGAN*[9]	51.02	0.094	-	-	43.86	0.299	-	-
SCGAN[7]	<b>20.38</b>	<b>0.068</b>	23.17	0.7535	<b>9.11</b>	0.205	21.56	0.7197
Ours	23.00	0.084	<b>24.78</b>	<b>0.7717</b>	11.89	<b>0.203</b>	<b>21.95</b>	<b>0.7377</b>

$$L_{cycle} = \mathbb{E} \| I_{LR}^{real} - DSNet(SNet(I_{LR}^{real})) \|_2^2 \quad (7)$$

To make the generated SR image conform to the distribution of the HR image, we apply the adversarial loss between  $I_{SR}^{SNet}$  and  $I_{HR}$ , the adversarial loss  $L_{adv}^{SNet}$  is similar with Eq. 4. Therefore, the overall loss function of SNet is:

$$L_{SNet} = \alpha_3 L_{rec}^{SNet} + \beta_3 L_{adv}^{SNet} + \gamma L_{cycle} \quad (8)$$

## 3. EXPERIMENTS

### 3.1. Experimental Setup

Following existing work SCGAN[7], we use the 20,000 high-quality, high-resolution face images from FFHQ dataset[15] and the 4,000 low-resolution face images from the Widerface[16] for training, and use two synthetic datasets, i.e., LS3D-W balanced[4] and FFHQ[15], and two real-world datasets, i.e., Widerface[16] and Webface[7] for testing. All the above datasets are processed in the same way as SCGAN[7]. All experiments were carried out at 4× super-resolution factor.

For quantitative evaluation, the non-reference metric FID [17] and full reference metrics (LPIPS [18], PSNR, and SSIM) are used for two synthetic datasets with corresponding high-resolution reference images. For two real-world datasets, the widely used metrics FID and NIQE [19] are used. The training process contains two stages. First, we separately train the degradation modeling down-sampling network, and set  $\alpha_1 = 1, \beta_1 = 0.05$ , and the batch size is set to 16. Then, we use the trained DeNet to generate its corresponding image from the HR image, which is close to the real LR image domain, for the second stage of training. In the second stage, we jointly train TNet and SNet with  $\alpha_2 = 1, \beta_2 = 0.001, \alpha_3 = 1, \beta_3 = 0.001, \gamma = 1$ . The batch size is set to 4. Canny and DoG edges are extracted based on the OpenCV library. The initial learning rate of all networks is set to  $1 \times 10^{-4}$ , halve every 10 epochs. And we use the ADAM optimizer [20] for training the model.

### 3.2. Comparisons with the state-of-the-art methods

We compare our proposed method with state-of-the-art SR methods, including generic SR methods like DASR[6], Real-ESRGAN[5], and face restoration methods like LRGAN[10],

**Table 2.** Quantitative comparison with state-of-the-art methods on two real-world datasets.

Methods	Widerface		WebFace	
	FID↓	NIQE↓	FID↓	NIQE↓
Bicubic	269.22	10.8979	273.46	11.2349
DASR[6]	102.79	8.5417	105.74	8.6894
Real-ESRGAN*[5]	41.73	6.7595	51.57	6.6773
LRGAN[10]	16.50	6.9084	23.23	7.0073
GFPGAN*[9]	59.34	6.9437	88.71	6.8841
SCGAN[7]	<b>13.05</b>	<b>6.6192</b>	<b>21.26</b>	<b>6.5835</b>
Ours	<u>14.31</u>	<b>6.0863</b>	<u>22.49</u>	<b>6.1948</b>

GFPGAN[9], SCGAN[7]. Bicubic interpolation is also introduced as a baseline. For a fair comparison, we use the same data as in SCGAN when training the models.

The quantitative results of different methods on the synthetic datasets are shown in Table 1. It can be observed that our method achieves the highest PSNR and SSIM on two datasets, and achieves the lowest LPIPS value on the FFHQ dataset. In addition, our FID on the two datasets also achieves the second-best and the competitive results with the method SCGAN [7], which shows that the results of our method can be well close to the distribution of real high-resolution face images and natural images while maintaining the pixel-level structure of the reference high-resolution images. The quantitative results of different methods on the synthetic datasets are shown in Table 2. It can be seen that our method obtains the lowest NIQE value and the second lowest FID value on the two datasets, indicating that the results obtained by our method can be very close to the distribution of real face images and natural images. It is worth noting that those ‘perceptual’ metrics are well correlated with the human-opinion-scores on a coarse scale, but not always well correlated on a finer scale [9].

Qualitative results on four datasets are shown in Fig. 3. It can be observed that our method is well consistent with the ground truth in terms of expression (such as the first column), skin color (such as the second column), and face structure and details. It also can be observed that, on real-world datasets, our method is more natural in the recovery of face structures (such as contours, eyes, mouth, etc.). In addition, combined with the results of LR images and Bicubic, it can be seen that ours is also better than LRGAN and SCGAN in terms of skin color and overall color restoration, which shows the necessity of our method to fully consider the domain gap.

### 3.3. Ablation study

To explore the effectiveness of each part of the proposed method, we further implement ablation studies on the FFHQ dataset and the Widerface dataset. First, the effect of introducing different edge information is analyzed. The baseline model (baseline) in this part means that no contour edge information (expressed in Canny) and Gaussian difference detail edge (expressed in DoG) are added. The quantitative results of the ablation study are shown in the upper part of Table 3. It can be seen that after gradually adding Canny and DoG, the metrics are gradually getting better.

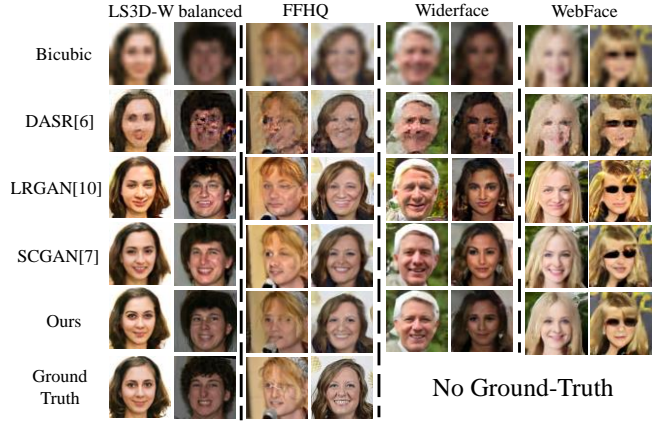


**Fig. 3.** Qualitative comparison with state-of-the-art methods on different datasets.

**Table 3.** Quantitative of different variant models.

Models	FFHQ				Widerface	
	FID↓	LPIPS↓	PSNR↑	SSIM↑	FID↓	NIQE↓
baseline	14.88	0.218	21.87	0.7323	15.51	6.6784
+Canny	12.34	0.214	21.72	0.7270	14.81	6.4855
+Canny+DoG(Ours)	<b>11.89</b>	<b>0.203</b>	<b>21.95</b>	<b>0.7377</b>	<b>14.31</b>	<b>6.0863</b>
Ours-cycle	41.62	0.245	20.52	0.6548	37.29	6.4345
Ours-w/o-cycle	13.65	0.209	21.88	0.7368	17.45	6.5511
Ours-TNet-bicubic	41.01	0.223	21.83	0.7295	39.84	8.2826
Ours-SNet-bicubic	20.92	<b>0.203</b>	21.58	0.7319	20.81	6.8400
Ours-TNet	15.06	0.212	<b>22.06</b>	<b>0.7522</b>	18.62	6.7601
Ours-SNet(Ours)	<b>11.89</b>	<b>0.203</b>	21.95	0.7377	<b>14.31</b>	<b>6.0863</b>

The effectiveness of each branch network: The quantitative results of all variants are shown in the lower part of Table 3. ‘Ours-cycle’ represents the TNet trained with cycle learning scheme [11], ‘Ours-w/o-cycle’ represents removing DSNet. The models trained with bicubic data are recorded as ‘Ours-TNet-bicubic’ and ‘Ours-SNet-bicubic’, and our final models are recorded as ‘Ours-TNet’ and ‘Ours-SNet’. From the results, we can observe the effectiveness of introducing the teacher-student training method and using the cycle consistency loss. Moreover, Ours-TNet obtained the highest PSNR and SSIM on the FFHQ test set.

## 4. CONCLUSION

This paper proposes a novel teacher-student FSR framework with the embedding of edge information, in which, the DeNet is used to synthesize LR data that approximates the real LR face image for the supervised training of the teacher super-resolution network. In addition, in order to facilitate the reconstruction of the overall structure and details of the face, we introduce edge information to explicitly make the network pay more attention to the recovery of high-frequency information. Extensive experiments have proved the superiority of our method and the effectiveness of all parts of the network.

## Acknowledgment

This work is supported by the National Natural Science Foundation of China (61503277) and the National Key Research and Development Program (2019YFE0198600).

## 5. REFERENCES

- [1] Cheng Ma, Zhenyu Jiang, Yongming Rao, Jiwen Lu, and Jie Zhou, “Deep face super-resolution with iterative collaboration between attentive recovery and landmark estimation,” in *Proceedings of the IEEE/CVF conference on computer vision and pattern recognition*, 2020, pp. 5569–5578.
- [2] Jonghyun Kim, Gen Li, Cheolkon Jung, and Joongkyu Kim, “Progressive face super-resolution with non-parametric facial prior enhancement,” in *2021 IEEE International Conference on Image Processing (ICIP)*. IEEE, 2021, pp. 899–903.
- [3] Chenggong Zhang and Zhilei Liu, “Face super-resolution with progressive embedding of multi-scale face priors,” in *2022 IEEE International Joint Conference on Biometrics (IJCB)*. IEEE, 2022, pp. 1–8.
- [4] Adrian Bulat and Georgios Tzimiropoulos, “How far are we from solving the 2d & 3d face alignment problem?(and a dataset of 230,000 3d facial landmarks),” in *Proceedings of the IEEE International Conference on Computer Vision*, 2017, pp. 1021–1030.
- [5] Xintao Wang, Liangbin Xie, Chao Dong, and Ying Shan, “Real-esrgan: Training real-world blind super-resolution with pure synthetic data,” in *Proceedings of the IEEE/CVF International Conference on Computer Vision*, 2021, pp. 1905–1914.
- [6] Yunxuan Wei, Shuhang Gu, Yawei Li, Radu Timofte, Longcun Jin, and Hengjie Song, “Unsupervised real-world image super resolution via domain-distance aware training,” in *Proceedings of the IEEE/CVF Conference on Computer Vision and Pattern Recognition*, 2021, pp. 13385–13394.
- [7] Hao Hou, Jun Xu, Yingkun Hou, Xiaotao Hu, Benzhen Wei, and Dinggang Shen, “Semi-cycled generative adversarial networks for real-world face super-resolution,” *IEEE Transactions on Image Processing*, 2023.
- [8] Kelvin CK Chan, Xintao Wang, Xiangyu Xu, Jinwei Gu, and Chen Change Loy, “Glean: Generative latent bank for large-factor image super-resolution,” in *Proceedings of the IEEE/CVF conference on computer vision and pattern recognition*, 2021, pp. 14245–14254.
- [9] Xintao Wang, Yu Li, Honglun Zhang, and Ying Shan, “Towards real-world blind face restoration with generative facial prior,” in *Proceedings of the IEEE/CVF Conference on Computer Vision and Pattern Recognition*, 2021, pp. 9168–9178.
- [10] Adrian Bulat, Jing Yang, and Georgios Tzimiropoulos, “To learn image super-resolution, use a gan to learn how to do image degradation first,” in *Proceedings of the European conference on computer vision (ECCV)*, 2018, pp. 185–200.
- [11] Jun-Yan Zhu, Taesung Park, Phillip Isola, and Alexei A Efros, “Unpaired image-to-image translation using cycle-consistent adversarial networks,” in *Proceedings of the IEEE international conference on computer vision*, 2017, pp. 2223–2232.
- [12] Xiang Wu, Ran He, Zhenan Sun, and Tieniu Tan, “A light cnn for deep face representation with noisy labels,” *IEEE Transactions on Information Forensics and Security*, vol. 13, no. 11, pp. 2884–2896, 2018.
- [13] Kaiming He, Xiangyu Zhang, Shaoqing Ren, and Jian Sun, “Deep residual learning for image recognition,” in *Proceedings of the IEEE conference on computer vision and pattern recognition*, 2016, pp. 770–778.
- [14] Zhen Li, Jinglei Yang, Zheng Liu, Xiaomin Yang, Gwanggil Jeon, and Wei Wu, “Feedback network for image super-resolution,” in *Proceedings of the IEEE/CVF Conference on Computer Vision and Pattern Recognition*, 2019, pp. 3867–3876.
- [15] Tero Karras, Samuli Laine, and Timo Aila, “A style-based generator architecture for generative adversarial networks,” in *Proceedings of the IEEE/CVF conference on computer vision and pattern recognition*, 2019, pp. 4401–4410.
- [16] Shuo Yang, Ping Luo, Chen-Change Loy, and Xiaoou Tang, “Wider face: A face detection benchmark,” in *Proceedings of the IEEE conference on computer vision and pattern recognition*, 2016, pp. 5525–5533.
- [17] Martin Heusel, Hubert Ramsauer, Thomas Unterthiner, Bernhard Nessler, and Sepp Hochreiter, “Gans trained by a two time-scale update rule converge to a local nash equilibrium,” *Advances in neural information processing systems*, vol. 30, 2017.
- [18] Richard Zhang, Phillip Isola, Alexei A Efros, Eli Shechtman, and Oliver Wang, “The unreasonable effectiveness of deep features as a perceptual metric,” in *Proceedings of the IEEE conference on computer vision and pattern recognition*, 2018, pp. 586–595.
- [19] Anish Mittal, Rajiv Soundararajan, and Alan C Bovik, “Making a “completely blind” image quality analyzer,” *IEEE Signal processing letters*, vol. 20, no. 3, pp. 209–212, 2012.
- [20] Diederik P Kingma and Jimmy Ba, “Adam: A method for stochastic optimization,” *arXiv preprint arXiv:1412.6980*, 2014.